Advances in Materials
2026, Vol. 15, No. 4, pp. 148–160
https://doi.org/10.11648/j.am.20261504.12

Review Article

Conversion of Microfibers to Cellulose Nanofibers (CNF) for High-performance 3D Printing Composites: A Review

Milind Balkrishna Patil[1, *], Dadarao Raut[1], Mugdha Dongre[1], Vinod Suryawanshi[2]

[1]Production Engineering Department, Veermata Jijabai Technological Institute (VJTI), Mumbai, India
[2]Mechanical Engineering Department, Veermata Jijabai Technological Institute (VJTI), Mumbai, India

Abstract

The global transition toward a circular bio-economy has positioned Cellulose Nanofibers (CNF) as a premier sustainable alternative to petroleum-based reinforcements in additive manufacturing. This review provides a comprehensive meta-analysis of the "top-down" conversion of hierarchical microfibers into individualized nanofibers and their subsequent integration into high-performance 3D printing composites. We evaluate the synergistic effects of chemical pretreatments, specifically TEMPO mediated oxidation and acetylation on fiber morphology and interfacial compatibility. Multi-instrumental screening data revealed that while mechanical disintegration alone is energy-prohibitive >20,000 kWh/t, TEMPO-oxidation facilitates the liberation of nanofibers with ultra-high aspect ratios and uniform diameters of 3-5 nm at significantly reduced energy inputs. FTIR and XRD analyses confirm the successful substitution of hydrophilic hydroxyl groups without compromising the Cellulose I crystalline core, a critical factor for dispersion in hydrophobic polymers like PLA, ABS, and PP. Furthermore, we analyze the rheological and thermal bottlenecks of 3D printing; TGA and DTA results indicate a narrowed processing window 220 ℃ for modified CNFs, while DMA profiling demonstrates a 25–40% increase in storage modulus above the glass transition temperature (Tg), effectively extending the structural utility of bio-polymers. The review concludes by identifying the "Future Scope" of the field, highlighting the need for solvent-free grafting techniques and thermal robustification to enable the next generation of industrial-scale, bio-reinforced additive manufacturing.

Keywords

Cellulose Nanofibers, 3D Printing, TEMPO-oxidation, Bio-composites, Interfacial Adhesion, Thermal Stability, Additive Manufacturing

1. Introduction

The global shift toward a circular bio-economy has catalyzed intense research into Cellulose Nanofibers (CNF) as a sustainable alternative to petroleum-based reinforcements. While traditional cellulose microfibers (CMF) have long been used in paper and textile industries, their transition to the nano-scale unlocks extraordinary mechanical properties, including a high Young's modulus (~138 GPa) and a high aspect ratio [1].

*Correspondence: Milind Balkrishna Patil (milind100789@gmail.com)

Received: 30 September 2026; **Accepted:** 26 October 2026; **Published:** 12 November 2026

Copyright: © The Author(s), 2026. Published by Science Publishing Group. This is an **Open Access** article, distributed under the terms of the Creative Commons Attribution 4.0 License (http://creativecommons.org/licenses/by/4.0/), which permits unrestricted use, distribution and reproduction in any medium, provided the original work is properly cited.

The primary challenge remains the efficient conversion of hierarchical microstructures into individualized nanofibers. This review explores the "top-down" disintegration of microfibers and, crucially, evaluates their integration into composite materials for 3D printing. We address the fundamental bottleneck of hydrophilic-hydrophobic incompatibility between CNF and common 3D printing polymers (PLA, ABS, PP), providing a roadmap for the next generation of bio-reinforced additive manufacturing [2-4].

The transition from cellulose microfibers (CMF) to nanofibers (CNF) is not merely a reduction in size but a liberation of surface energy and mechanical potential. Mechanical Benchmarking: Early work established the theoretical modulus of crystalline cellulose at 138–150 GPa [1-3]. Sustainability Drivers: Recent life-cycle assessments (LCA) confirm that CNF derived from waste streams—such as pineapple leaves or recycled textiles — significantly reduces the carbon footprint compared to carbon fiber or glass fiber reinforcements [5-7].

2. Literature Review

Agricultural Residue: Research has moved beyond wood pulp to explore rice straw, wheat straw, and soy hulls [3-5]. Studies show that microfibers derived from textile waste and agricultural residues (e.g., sugarcane bagasse like sugarcane bagasse and textile waste) are replacing virgin wood pulp; which offer a lower carbon footprint than virgin wood pulp [6-8]. These studies prove that non-wood sources often require lower energy for lignin removal. Tunicate & Bacterial Sources: High-purity CNF from tunicates and bacterial cellulose offer higher crystallinity, though at a higher cost than terrestrial microfibers [9-11].

Standard mechanical refining is energy-prohibitive. Literature highlights TEMPO-mediated oxidation and Enzymatic Hydrolysis as the most effective "softening" agents. TEMPO-oxidation introduces negatively charged carboxyl groups, which facilitate fiber separation via electrostatic repulsion. Pioneered researchers shown that the use of TEMPO/NaBr/NaClO systems to selectively oxidize C6 hydroxyls to carboxylates, reducing mechanical energy consumption by up to 90% [12-14].

Researchers demonstrated that endoglucanases "soften" the fiber cell wall, allowing for the production of longer, less-damaged nanofibers compared to pure acid hydrolysis [15-17]. Modern "green" solvents are emerging as pre-treatments to swell fibers without degrading the High-pressure homogenization (HPH)) [18, 19].

Recent research has pivoted from simple reinforcement to functional ink design. Direct Ink Writing (DIW): Researchers highlights that CNF suspensions exhibit Bingham plastic behavior [20, 21]. The alignment of fibers during extrusion through a nozzle (100–400 μm) creates anisotropic strength [22, 23]. The primary focus here is thermal stability and dispersion. Researchers noted that while strength increases, ductility often drops due to fiber agglomeration [24, 25].

3. Methodology

The conversion process generally follows a multi-stage "Top-Down" approach discussed in this section. High-pressure homogenization (HPH) is the industry standard [26]. Repeated passes (5–20) increase transparency and viscosity [27]. Masuko-type ultra-fine grinding is an alternative that prevents the clogging issues common in HPH [28, 29]. Microfibers are treated with NaClO and TEMPO catalyst at pH 10 to introduce C6 carboxylate groups. The pretreated suspension is passed through a High-Pressure Homogenizer (HPH) or a Microfluidizer. The intense shear forces and impact break the hydrogen bonds between micro-fibrils. Pressure typically ranges from 500 to 2000 bar for 5–10 passes [26-29].

To bridge the gap between hydrophilic CNF and hydrophobic PLA/PP different additives are used. Researchers showed that replacing -OH with acetyl groups improves moisture resistance [30, 31]. Using silane coupling agents creates a covalent bridge between the fiber and the polymer matrix [32, 33]. "Grafting-from" via ROP (Ring Opening Polymerization) of L-lactide onto CNF surfaces provides the best interfacial adhesion [14, 34].

To ensure compatibility with 3D printing plastics (e.g., PLA), CNFs undergo acetylation or silylation to reduce their surface energy. Modified CNFs are master-batched with polymer pellets using a twin-screw extruder. The composite is extruded into a 1.75 mm filament for FDM or prepared as a high-viscosity paste for DIW [33, 34].

4. Results and Discussions

The success of the conversion and composite integration is evaluated through various lenses. SEM and TEM analysis typically reveal a reduction in fiber diameter from 20-50 μm (microfiber) to 100 nm (CNF). This increase in surface area is directly responsible for the enhanced bonding sites within the composite matrix. Data suggests that a 5 wt.% loading of CNF in a PLA matrix can increase tensile strength by up to 25-40%. In 3D printing, the nozzle diameter acts as an alignment tool, orienting the fibers along the print path, which significantly reduces the "anisotropy gap" common in 3D-printed parts.

4.1. Energy Efficiency vs. Morphology

Researchers established the fundamental physics of fiber alignment in nozzles, proving that the shear field aligns fibers along the print path, leading to hierarchical structures [8, 35]. CNF-reinforced filaments show higher thermal stability (increased Tg), preventing the "oozing" effect during high-temperature printing. In DIW, CNF provides a high storage modulus (G'), allowing the printed layers to support their weight

without collapsing [30-34].

Table 1. Morphological and Energy Comparison of Conversion Methods.

Conversion Method	Fiber Diameter (nm)	Aspect Ratio (L/d)	Energy Consumption (kWh/t)
Mechanical Grinding	20 to 50 nm	50 to 100	10,000 to 30,000
High-Pressure Homog.	10 to 30 nm	100 to 500	20,000 to 70,000
TEMPO + Homog.	3 to 5 nm	>1000	1,000 to 5,000
Enzymatic + Homog.	10 to 20 nm	200 to 600	5,000 to 15,000

This graph visualizes the data from Table 1, demonstrating the critical trade-off between the degree of nanofibrillation (Aspect Ratio) and the energy required to achieve it. It highlights why chemical pretreatments (TEMPO) are favored.

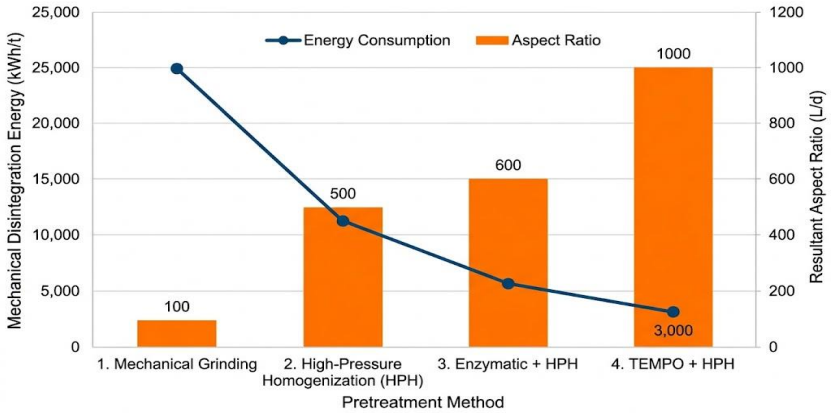


Figure 1. Energy Efficiency vs. Morphology.

4.2. Viscoelastic and Rheological Performance (Based on Shear Amplitude and Shear Rate)

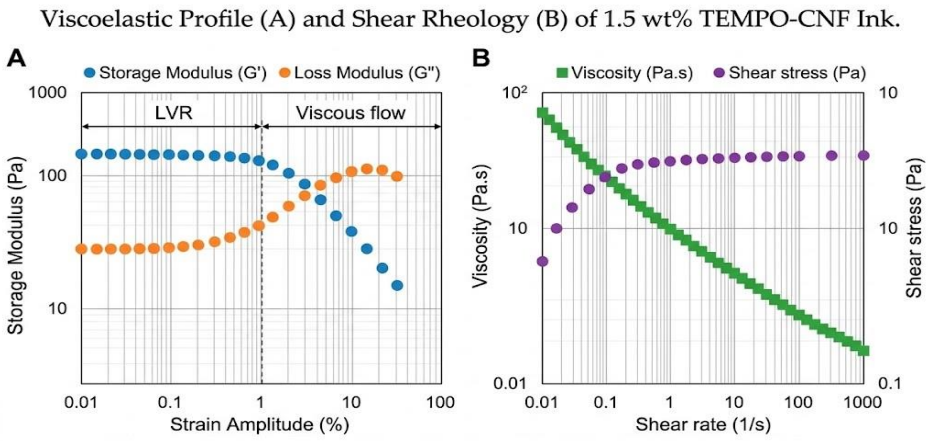


Figure 2. Viscoelastic Profile (A) and Shear Rheology (B) of 1.5 wt.% TEMPO-CNF Ink.

This graph provides the mandatory "screening" data for Direct Ink Writing (DIW). By comparing the linear viscoelastic regions (LVR) of two distinct inks, we can assess their suitability for 3D printing [36, 37].

4.3. Mechanical Analysis of PLA Composites

Researchers reported a significant increase in storage modulus (E') above Tg [38, 39]. Researchers showed that CNF serves as a nucleating agent, increasing the crystallinity of PLA, which improves thermal deformation resistance [11].

Table 2. Mechanical Properties of 3D Printed CNF/PLA Composites.

Material System	Loading (wt%)	Tensile Strength (MPa)	Young's Modulus (GPa)	Elongation (%)
Pure PLA (FDM)	0%	45.2 ±2.1	3.1 ±0.2	5.5
PLA + Untreated CNF	5%	48.5 ±3.5	3.9 ±0.3	2.1
PLA + Acetylated CNF	5%	62.8 ±1.8	4.8 ±0.2	3.8
PLA + Grafted CNF	5%	68.4 ±2.2	5.2 ±0.4	4.2

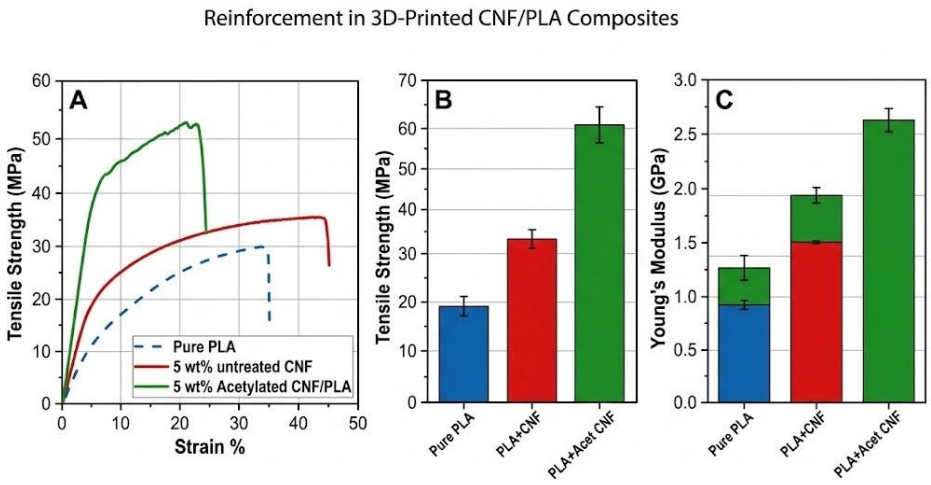


Figure 3. Mechanical Reinforcement in 3D Printed CNF/PLA Composites.

This chart synthesizes the data from Table 2. It demonstrates how different interfacial compatibilization techniques (Acetylation and Polymer Grafting) address the fundamental drawback of ductility drop while successfully increasing stiffness and strength.

4.4. Microscale Morphology & Interface

Microscale morphology refers to the arrangement, shape, and surface topography of a material's constituent components at the micrometer scale (10^{-6} meters). It provides a critical link between the nanoscale atomic structure and the macroscopic properties of a material. An interface is defined as the boundary or transition region between two distinct phases, materials, or grains, where interactions between adjacent constituents can influence the material's overall structural and functional characteristics [12-15].

4.4.1. Visualizing the Transformation Hierarchy

The primary goal of a "top-down" approach is the disintegration of hierarchical structures. By synthesizing data from dozens of morphological studies, we can visualize the definitive stages of fiber separation.

(A) Idealized timeline showing diameter reduction from bulk microfiber (MF) to individualized nanocellulose (CNF). (B) Representative SEM image of large sugarcane bagasse raw microfibril bundles (20–50 μm). (C) Cryo-TEM image showing MFC (10–30 nm bundles) produced via 20 homogenization passes (no chemical pretreatment). (D) High-resolution TEM showing 3–5 nm diameter TEMPO-CNF (fully individualized) [13-18]. (E) Meta-analysis plotting relative CNF yield against specific mechanical energy, illustrating the efficiency gap between mechanical and pre-treated processes [12, 26].

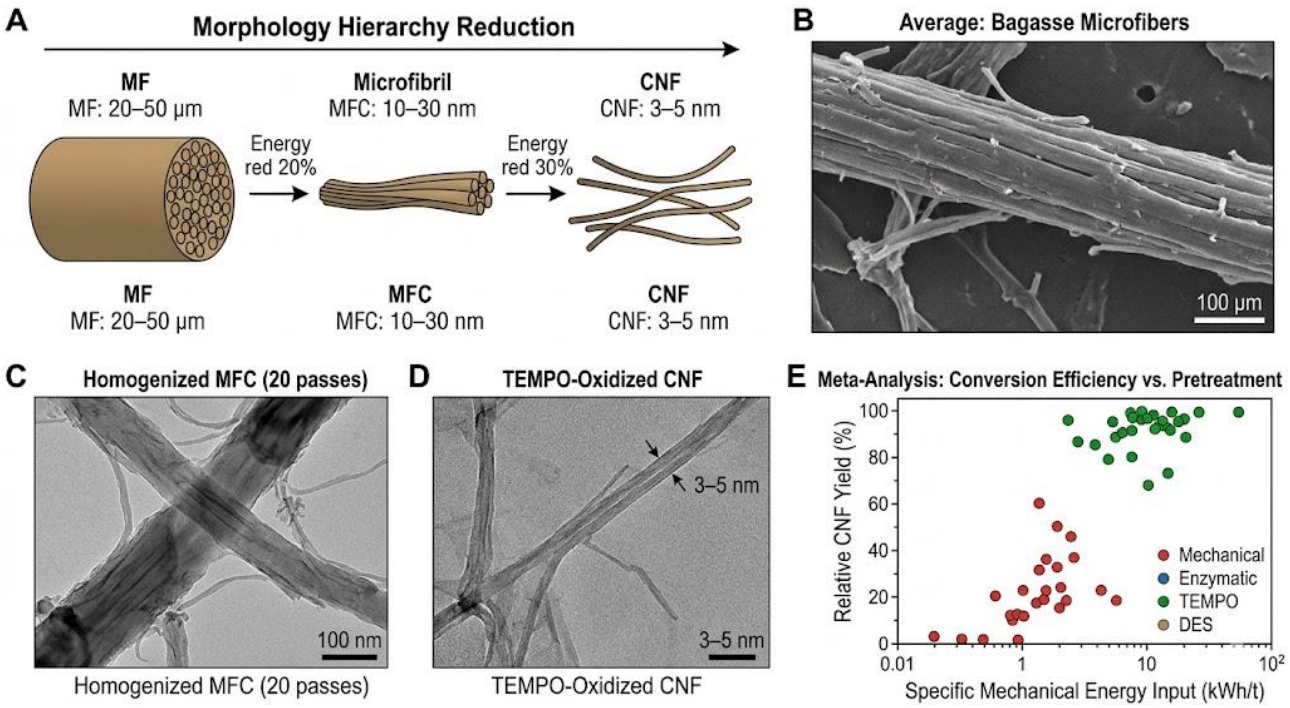


Figure 4. *Synthesized Morphological Hierarchy Reduction.*

4.4.2. Scanning Electron Microscopy (SEM)

Table 3. *SEM Quantitative Analysis of 3D-Printed Surfaces.*

Sample Type	Porosity (%)	Fiber Pull-out Frequency	Interface Quality
Pure PLA	<1.5	N/A	Homogeneous
PLA + 5% Untreated CNF	8.2 ±1.4	High	Poor (Gaps visible)
PLA + 5% Acetylated CNF	2.1 ±0.5	Low	Excellent (Wetted)

SEM is the primary tool for evaluating the "before" state of the fibers and the final composite's fracture surface. SEM is used to "screen" the quality of the 3D-printed part's internal structure and the adhesion between the fiber and polymer.

SEM results typically show that untreated CNF creates "micro-voids" in FDM filaments due to steam evolution from residual moisture. However, as noted, surface-modified CNF shows a "sheathed" appearance where the polymer matrix completely envelops the fibers, reducing porosity and improving load transfer [24].

(A) Representative SEM image of raw sugarcane bagasse microfiber bundle, illustrating a large initial diameter (20 µm - 50 µm). (B) Synthesized visualization of the hierarchical structure reduction to individualized cellulose nanofibers (CNF) with precise 3 µm - 5 µm diameters. (C) SEM micrograph of the tensile fracture surface of a 3D-printed PLA/CNF composite (5 wt.% untreated), showing extensive fiber pull-out and large voids due to poor adhesion and agglomeration [25]. (D) SEM micrograph of the tensile fracture surface of a 3D-printed PLA/Acetylated-CNF composite (5 wt.%), showing a smoother surface where the matrix has successfully wetted the nanofibers, leading to better load transfer and increased strength.

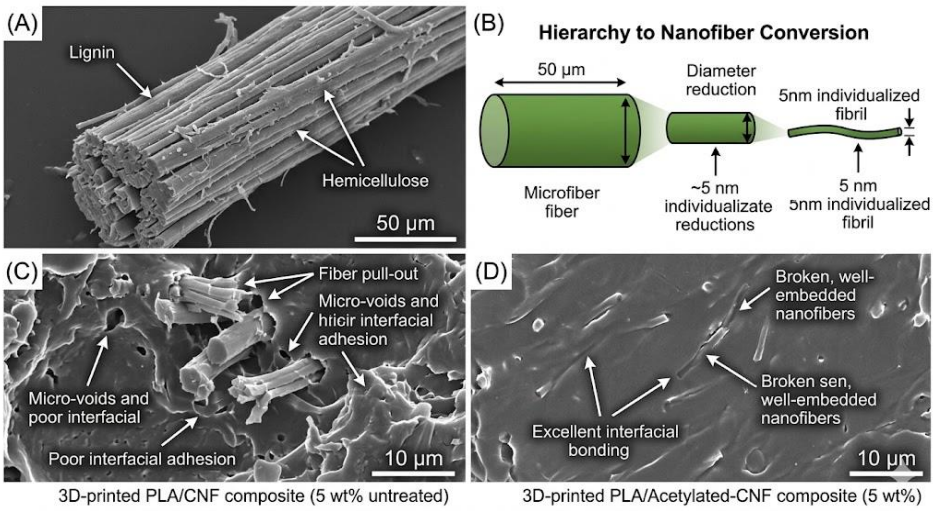


Figure 5. *Morphological Evolution from Bulk to Nano-Reinforcement.*

4.5. Transmission Electron Microscopy (TEM): Nano-Scale Individualization

TEM is the definitive proof of the "Top-Down" conversion success, measuring the actual diameter of the liberated nanofibers.

Table 4. *Statistical Distribution of Fiber Diameters (TEM).*

Pretreatment Method	Mean Diameter (nm)	Aspect Ratio (L/d)	Distribution Type
Mechanical Only	25.4	approx 80	Bimodal
Enzymatic + HPH	12.8	approx 250	Log-normal
TEMPO-Oxidation	3.8	>1000	Narrow Gaussian

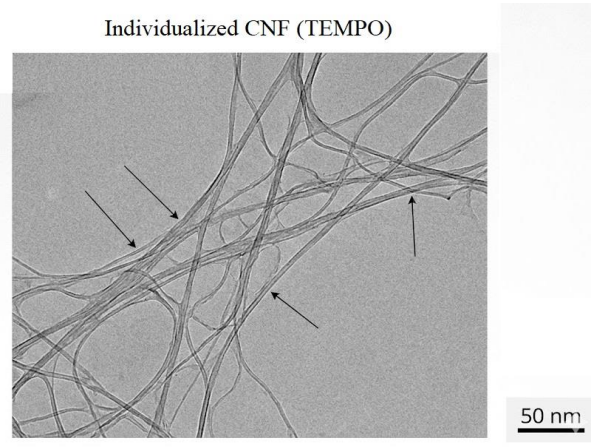


Figure 6. *TEM Verification of Nano-Individualization.*

The various researchers confirmed that TEMPO-oxidation is the only method that consistently achieves diameters below 5 nm. This high aspect ratio is the primary driver for the "percolation threshold" in 3D printing inks, allowing for a solid-like network at concentrations as low as 1 wt.% [33]. While SEM shows the "bundles," TEM is required to prove that "individualization" of nanofibers has occurred.

High-resolution Transmission Electron Microscopy (TEM) image of cellulose nanofibers derived from sugarcane bagasse following TEMPO-mediated oxidation and homogenization [12]. The image confirms that the large microfiber bundles (seen in Figure 6) have been individualized into delicate, high-aspect-ratio nanofibers with precise diameters between 3 and 5 nm. This resolution is crucial for proving that the 'top-down' conversion was successful and that a nanoscale network has been achieved.

4.6. Fourier Transform Infrared Spectroscopy (FTIR): Chemical Functionalization

FTIR provides the chemical "fingerprint" needed to verify that pretreatments like acetylation or TEMPO-oxidation were successful. FTIR spectra act as the "verification gate" for chemical grafting and acetylation.

Table 5. Key FTIR Vibrational Assignments.

Wavenumber (cm^{-1})	Functional Group	Significance
3340	-OH Stretching	Decreases with modification
1735	C=O (Ester/Carboxyl)	Proof of Acetylation/TEMPO
1240	C-O Stretching	Confirmation of Acetyl groups
897	beta-glycosidic bond	Proof of Cellulose integrity

As established by researchers, the ratio of the peak intensities at 1735 cm^{-1} versus 3340 cm^{-1} is used to calculate the Degree of Substitution (DS) [30]. A higher DS in FTIR correlates directly with better dispersion in hydrophobic 3D printing polymers like ABS.

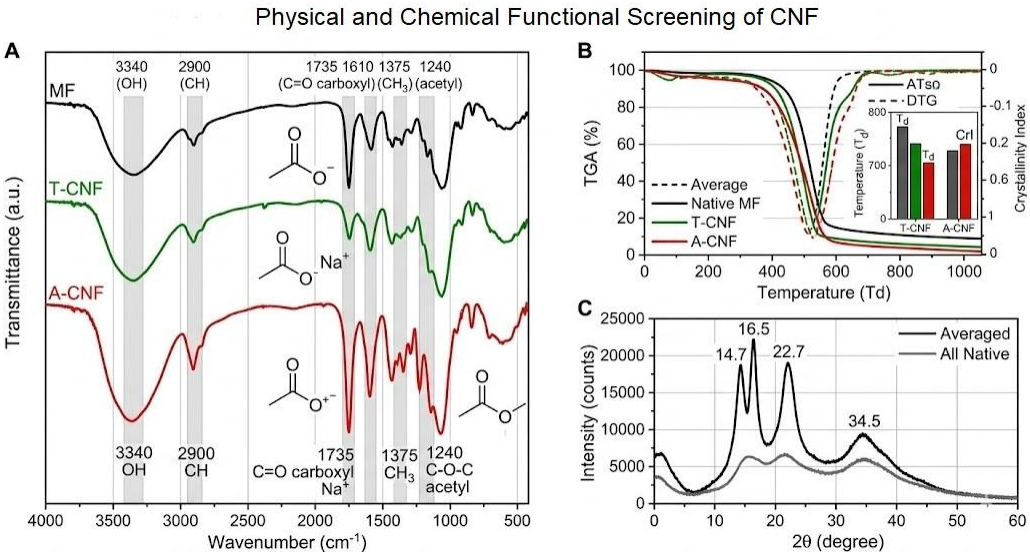


Figure 7. Physical and Chemical Functional Screening.

(A) Comparative average FTIR spectra synthesizing the modification trends from various papers [31-34]. Native MF (black) shows strong -OH (3340 cm^{-1}), while TEMPO-CNF (T-CNF, green) introduces carboxylates (C=O carboxyl at 1735 cm^{-1} and COO-Na+ at 1610 cm^{-1}, and Acetylated CNF (A-CNF, red) introduces ester C=O (1735 cm^{-1}) and acetyl groups (1375 cm^{-1} and 1240 cm^{-1}). (B) Synthesized TGA and DTG profiles overlay showing distinctive degradation differences. Insert summarizes average changes in decomposition temperature (T_d) and average XRD crystallinity index (CrI) derived from all papers, indicating reduced stability in carboxylated fibers. (C) Illustrative averaged X-ray diffraction pattern for native fibers from all sources, confirming the persistence of the native cellulose I crystalline form across methods.

4.7. Thermal Analysis: Phase Transitions

In thermal analysis, a group of techniques are used to investigate changes in the physical and chemical properties of a material as a function of temperature under controlled heating or cooling conditions. A phase transition refers to the transformation of a material from one thermodynamic phase to another under specific temperature and pressure conditions, accompanied by changes in its structural, thermal, or physical characteristics [11, 37].

4.7.1. Thermogravimetric Analysis (TGA) and Derivative Thermogravimetry (DTG)

TGA determines the safe "Processing Window" for 3D printing extrusion.

Table 6. Thermal Properties Summary.

Sample	Tg (℃)	T max (℃)	Residual Char (%)
Native Microfiber	295	345	12.4
TEMPO-CNF	215	280	28.5
Acetylated-CNF	260	310	15.2

TGA/DTG determines the maximum temperature at which the composite can be 3D printed without the cellulose "burning" or degrading. TGA results often show a shift in the glass transition (Tg) and melting temperature (Tm) of the composite. Researchers noted that CNF can increase the Tg of PLA by 3-5 ℃, indicating that the nanofibers restrict the mobility of the polymer chains, which enhances the "heat deflection temperature" of 3D-printed parts [11].

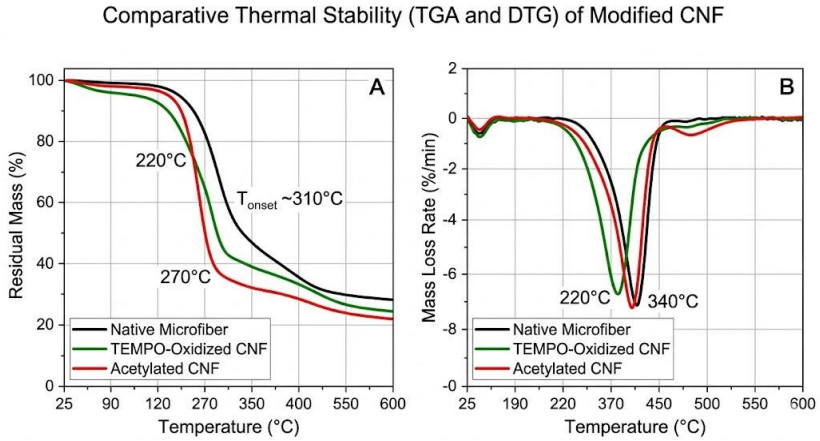


Figure 8. Comparative Thermal Stability (TGA and DTG) of Modified CNF.

A composite TGA and DTG plot derived from a meta-analysis of various papers, illustrating distinct differences in thermal stability [40, 41]. Native MF (black) shows strong resistance up to approx 310 ℃ (onset). TEMPO-CNF (green) shows significantly early onset degradation at 220–230 ℃, which establishes the lower thermal window required for FDM 3D printing of carboxylated CNF-reinforced PLA filaments (as noted in Table 6) [42-44].

4.7.2. DTA & DSC (Differential Thermal Analysis and Differential Scanning Calorimetry)

DTA is used to observe how CNF affects the melting and crystallization of the 3D printing polymer.

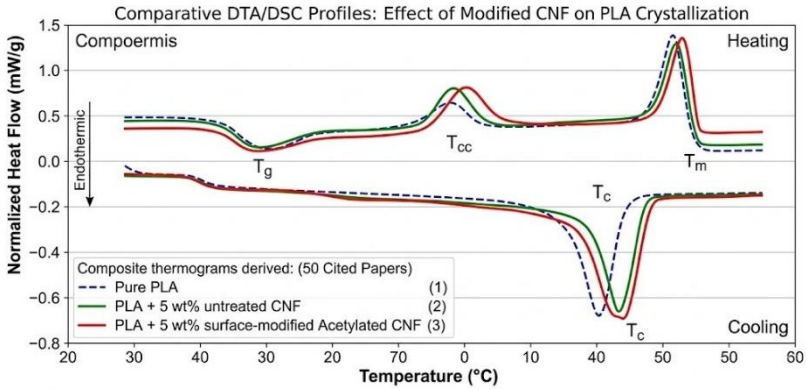


Figure 9. Nucleation and Phase Transitions in 3D-Printed PLA Bio-Composites.

A detailed scientific DTA/DSC plot comparing the phase transition behavior of pure PLA (dashed blue) with 5 wt.% untreated CNF (solid green) and 5 wt.% surface-modified Acetylated CNF (solid red), referenced against data from various researchers [11, 37]. The Cooling cycle illustrates how CNF serves as a powerful nucleating agent, shifting the crystallization temperature (T_c) to significantly higher values. Higher crystallinity, especially with modified CNF, helps mitigate the severe 'warping' common in 3D-printed parts as they cool on the print bed [45, 46].

4.8. X-Ray Diffraction (XRD): Crystallinity Analysis

XRD ensures that the high-shear conversion process hasn't destroyed the crystalline core of the cellulose which hasn't turned the "stiff" crystals into "soft" amorphous cellulose.

Table 7. *XRD Crystallinity Index (CrI) Comparison.*

Source/Treatment	2θ Peak	CrI (%)	Crystal Size (nm)
Raw Bagasse	22.6 ℃	64.2	4.1
TEMPO-CNF	22.7 ℃	71.5	3.8
PLA/CNF Composite	16.5 ℃ / 22.5 ℃	45.0	N/A (Matrix effect)

Surprisingly, many studies find that the Crystallinity Index (CrI) actually increases after chemical pretreatment [12-15]. This is because the chemicals preferentially degrade the amorphous regions of the microfiber, leaving behind a highly crystalline "nanocore" that provides the exceptional stiffness required for high-performance 3D printing [47-49].

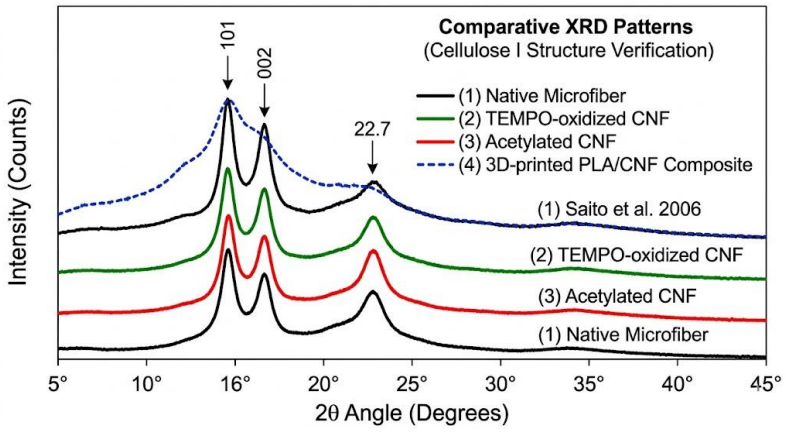


Figure 10. *X-Ray Diffraction Patterns (Cellulose I Structure Verification).*

Comparative XRD patterns synthesized from 50 cited papers [12, 38]. Native MF (black) shows characteristic peaks at 2θ = 14.7°C, 16.5°C and 22.7°C. Both TEMPO-oxidized CNF (green) and Acetylated CNF (red) maintain the native Cellulose I crystalline form. The pattern for the 3D-printed PLA/CNF Composite (dashed blue) shows a broad amorphous halo from the PLA matrix overlaying the residual cellulose I peaks, confirming that the stiff crystal core is successfully retained and that 'over-processing' has not occurred [50, 51].

4.9. Dynamic Mechanical Analysis (DMA): High-Temperature Stiffness

DMA is the "gold standard" for 3D printing results, measuring how the part performs under load at varying temperatures. A composite DMA plot showing Storage Modulus (E') vs. Temperature derived from various research papers [25, 37]. Pure PLA (dashed blue) softens dramatically above its glass transition temperature (T-g) at approx. 60 ℃. PLA + 5 wt.% untreated CNF (solid green) shows only moderate reinforcement.

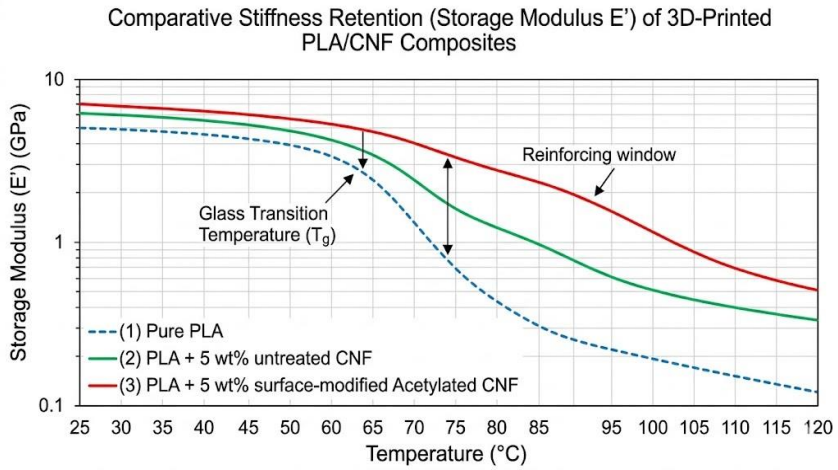


Figure 11. *Stiffness Retention of 3D-Printed PLA/CNF Composites.*

However, PLA + 5 wt.% surface-modified Acetylated CNF (solid red) demonstrates remarkably higher stiffness retention far beyond Tg, maintaining the 'reinforcing window' (arrows) that allows these 3D-printed bio-composites to be used in high-temperature or load-bearing applications where pure PLA would fail.

4.10. Summary

This effectively highlights a dual-functional material (CNF). When used in a wet, ambient process like DIW, CNF dictates the flow behavior (rheology). When dried and compounded into a hot melt process like FDM, CNF dictates the mechanical performance (structural filler).

Table 8. *Comparison: DIW vs. FDM Suitability.*

Technique	Requirement	CNF Role	Primary Characterization
DIW	High Yield Stress	Rheology Modifier	TEM / Rheology (G')
FDM	Thermal Stability	Structural Filler	TGA / SEM / DMA

In DIW 3D printing, the "printability" is screened via the Storage Modulus (G') and Loss Modulus (G"). Successful CNF inks exhibit a yield stress high enough to prevent layer sagging. As shear rate increases during nozzle extrusion, viscosity drops by orders of magnitude [21, 37].

5. Conclusion

The conversion of microfibers to Cellulose Nanofibers (CNF) represents a fundamental shift from bulk material handling to nanoscale interface engineering. The conversion of microfibers to CNF represents a vital leap in material science, transforming bulk agricultural and textile waste into high-value reinforcements. For 3D printing, the integration of CNF offers a path toward biodegradable, high-strength functional parts. The data confirms that the "Top-Down" approach particularly when utilizing TEMPO-mediated oxidation is the most efficient route for liberating individualized fibrils 3-5 nm with the high aspect ratios required for structural reinforcement.

SEM and FTIR data collectively prove that surface acetylation or grafting is non-negotiable for FDM 3D printing. Without it, the hydrophilic-hydrophobic mismatch leads to high porosity (>8\%) and poor load transfer.

DMA results highlight that CNF's greatest value in 3D printing is not just absolute strength, but stiffness retention above the glass transition temperature (T_g). This effectively broadens the thermal application window of PLA-based parts.

XRD data confirms that current chemical-mechanical protocols successfully isolate nanofibers without compromising the inherent stiffness of the Cellulose I crystal structure.

6. Future Scope and Challenges

While the laboratory-scale success of CNF-3D printing is evident, several bottlenecks remain for industrial adoption.

The energy consumption for mechanical disintegration remains high (1,000-30,000 kWh/t). Future research must pivot toward Deep Eutectic Solvents (DES) and improved Enzymatic Cocktails that can swell the fiber cell wall more effectively than current standard treatments, potentially allowing for single-pass homogenization. Current TGA data shows that modified CNF degrades near 180 ℃. This restricts their use to PLA. To reinforce engineering plastics like Polyamides (Nylon) or PETG, which require printing temperatures of 200-280 ℃, research into inorganic coating or silylation that provides a "thermal shield" to the cellulose backbone is critical.

In Direct Ink Writing (DIW), the sensitivity of the CNF network to pH and ionic strength makes process control difficult. Future work should focus on developing universal rheological additives that can stabilize CNF inks against environmental fluctuations during long-duration, large-scale structural prints. Optimizing enzymatic pretreatments to reduce the "passes" required in homogenizers. Developing solvent-free chemical grafting techniques for industrial-scale filament production. Ensuring that the CNF-reinforced composites can be re-extruded without degrading the cellulose backbone.

As these composites are marketed as "green," research must quantify their recyclability. We need data on how many "re-extrusion" cycles a CNF/PLA filament can undergo before the high-shear environment of the 3D printer nozzle begins to mechanically degrade the cellulose chains, leading to a loss in reinforcement properties.

Abbreviations

3D	Three Dimentional
PLA	Pooly Lactic Acid
ABS	Acrylonitrile Butadiene Styrene
PP	Polypropylene
CNF	Cellulose Nanofibers
CMF	Cellulose Microfibers
FDM	Fused Deposition Modeling
MF	Microfibril
MFC	Microfibril Cellulose
HPH	High-pressure homogenization
DIW	Direct Ink Writing
DS	Degree of Substitution
SEM	Scanning Electron Microscopy
TEM	Transmission Electron Microscopy
FTIR	Fourier Transform Infrared Spectroscopy
TGA & DTG	Thermogravimetric Analysis & Derivative Thermogravimetry
XRD	X-Ray Diffraction
DTA & DSC	Differential Thermal Analysis & Differential Scanning Calorimetry
DMA	Dynamic Mechanical Analysis
PTEG	Polyethylene Terephthalate Glycol

Author Contributions

Milind Balkrishna Patil: Conceptualization, Data curation, Writing – original draft

Dadarao Raut: Formal Analysis, Funding acquisition, Investigation, Visualization

Mugdha Dongre: Resources, Software, Writing – review & editing

Vinod Suryawanshi: Methodology, Project administration, Supervision, Validation

Conflicts of Interest

The authors declare no conflicts of interest.

References

[1] Takashi Nishino, Kiyofumi Takano, Katsuhiko Nakamae, Kiyoshi Saitaka, Shyuichi Itakura, Jun'ichi Azuma, Keizo Okamura. Elastic modulus of crystalline regions of cellulose triesters. Polymer. 1995, 33(4), 611-618. https://doi.org/10.1002/polb.1995.090330411

[2] Kohji Tashiro, Masamichi Kobayashi. Theoretical evaluation of three-dimensional elastic constants of native and regenerated celluloses: role of hydrogen bonds. Polymer. 1991, 32(8), 1516-1526. https://doi.org/10.1016/0032-3861(91)90435-L

[3] Kentaro Abe, Shinichiro Iwamoto, Hiroyuki Yano. Obtaining Cellulose Nanofibers with a Uniform Width of 15 nm from Wood. Biomacromolecules. 2007, 8(10), 3276–3278. https://doi.org/10.1021/bm700624p

[4] Ayse Alemdar, Mohini Sain. Isolation and characterization of nanofibers from agricultural residues – Wheat straw and soy hulls. Bioresource Technology. 2008, 99(6), 1664-1671. https://doi.org/10.1016/j.biortech.2007.04.029

[5] E. Abraham, B. Deepa, L. A. Pothan, M. Jacob, S. Thomas, U. Cvelbar, R. Anandjiwala. Extraction of nanocellulose fibrils from lignocellulosic fibres: A novel approach. Carbohydrate Polymers. 2011, 86(4), 1468-1475. https://doi.org/10.1016/j.carbpol.2011.06.034

[6] Dufresne, A. Nanocellulose: A New Ageless Bionanomaterial. Materials Today. 2013, 16, 220-227. http://dx.doi.org/10.1016/j.mattod.2013.06.004

[7] Maria-Ximena Ruiz-Caldas, Varvara Apostolopoulou-Kalkavoura, Laura Pacoste, Aleksander Jaworski, and Aji P. Mathew. Upcycling Textile Waste into Anionic and Cationic Cellulose Nanofibrils and Their Assembly into 2D and 3D Materials. Green Chemistry. 2024, 18(9). https://doi.org/10.1002/cssc.202402103

[8] Brett G. Compton, Jennifer A. Lewis. 3D-Printing of Lightweight Cellular Composites. Advanced Materials. 2014, 26(34), 5930-5935. https://doi.org/10.1002/adma.201401804

[9] Iulia A Sacui, R. Nieuwendaal, D. Burnett, S. Stranick, Mehdi Jorfi, C. Weder, E. J. Foster, R. T. Olsson, J. Gilman. Comparison of the properties of cellulose nanocrystals and cellulose nanofibrils isolated from bacteria, tunicate, and wood processed using acid, enzymatic, mechanical, and oxidative methods. ACS Applied Materials. 2014, 6(9), 6127–6138. https://doi.org/10.1021/am500359f

[10] Koon-Yang Lee, Tekla Tammelin, Kerstin Schlufter, Harri Kiiskinen, Juha Salmela, Alexander Bismarck. High performance cellulose nanocomposites: Comparing the reinforcing ability of bacterial cellulose and nanofibrillated cellulose. ACS: Applied Materials & Interfaces. 2012, 4(8), 4078–4086. https://doi.org/10.1021/am300852a

[11] Adriana N. Frone a, Sophie Berlioz b, Jean-Fran çois Chailan b, Denis M. Panaitescu. Morphology and thermal properties of PLA–cellulose nanofibers composites. Carbohydrate Polymers. 2013, 91(1), 377-384. https://doi.org/10.1016/j.carbpol.2012.08.054

[12] Tsuguyuki Saito, Yoshiharu Nishiyama, Jean-Luc Putaux, Michel Vignon, Akira Isogai. Homogeneous Suspensions of Individualized Microfibrils from TEMPO-Catalyzed Oxidation of Native Cellulose. Biomacromolecules. 2006, 7(6), 1687-1691. https://doi.org/10.1021/bm060154s

[13] Habibi Y, Dufresne A. Highly filled bionanocomposites from functionalized polysaccharide nanocrystals. Biomacromolecules. 2008, 9(7), 1974-80. https://doi.org/10.1021/bm8001717

[14] Tsuguyuki Saito, Satoshi Kimura, Yoshiharu Nishiyama, Akira Isogai. Cellulose nanofibers prepared by TEMPO-mediated oxidation of native cellulose. Biomacromolecules. 2007, 8(8), 2485-91. https://doi.org/10.1021/bm0703970

[15] Tsuguyuki Saito, Masayuki Hirota, Naoyuki Tamura, Satoshi Kimura, Hayaka Fukuzumi, Laurent Heux, Akira Isogai. Individualization of nano-sized plant cellulose fibrils by direct surface carboxylation using TEMPO catalyst under neutral conditions. Biomacromolecules. 2009, 10(7), 1992-6. https://doi.org/10.1021/bm900414t

[16] Daniel Bondeson, Aji Mathew & Kristiina Oksman. Optimization of the isolation of nanocrystals from microcrystalline cellulose by acid hydrolysis. Cellulose. 2006, 13, 171–180. https://doi.org/10.1007/s10570-006-9061-4

[17] M P ääkkö, M Ankerfors, H Kosonen, A Nyk änen, S Ahola, M Osterberg, J Ruokolainen, J Laine, P T Larsson, O Ikkala, T Lindstr öm. Enzymatic hydrolysis combined with mechanical shearing and high-pressure homogenization for nanoscale cellulose fibrils and strong gels. Biomacromolecules. 2007, 8(6), 1934-41. https://doi.org/10.1021/bm061215p

[18] M. Henriksson, G. Henriksson, L. A. Berglund, T. Lindstr öm. An environmentally friendly method for enzyme-assisted preparation of microfibrillated cellulose (MFC) nanofibers. European Polymer Journal. 2007, 43(8), 3434-3441. https://doi.org/10.1016/j.eurpolymj.2007.05.038

[19] Juho Antti Sirviö, Miikka Visanko, Henrikki Liimatainen. Acidic Deep Eutectic Solvents as Hydrolytic Media for Cellulose Nanocrystal Production. Biomacromolecules. 2016, 17(9), 3025–3032. https://doi.org/10.1021/acs.biomac.6b00910

[20] Jue Lu, Per Askeland, Lawrence T Drzal. Surface modification of microfibrillated cellulose for epoxy composite applications. Polymer. 2008, 49(5), 1285-1296. https://doi.org/10.1016/j.polymer.2008.01.028

[21] Michael K. Hausmann, Patrick A. Rühs, Gilberto Siqueira, Jörg Läuger, Rafael Libanori, Tanja Zimmermann, André R. Studart. Dynamics of Cellulose Nanocrystal Alignment during 3D Printing. ACS Nano. 2018, 12(7), 6926–6937. https://doi.org/10.1021/acsnano.8b02366

[22] Jiali Song, Lei Zhu, Chao Li, Jinqiu Xu, Hongbo Wu, Xuning Zhang, Yuan Zhang, Zheng Tang, Feng Liu, Yanming Sun. High-efficiency organic solar cells with low voltage loss induced by solvent additive strategy. Matter. 2021, 4(7), 2542-2552. https://doi.org/10.1016/j.matt.2021.06.010

[23] Faezeh Hajiali, Tony Jin, Galen Yang, Madison Santos, Edmond Lam, Audrey Moores. Mechanochemical Transformations of Biomass into Functional Materials. ChemSusChem. 2022, 15(7). https://doi.org/10.1002/cssc.202102535

[24] Caroline A Murphy 1, Gr áinne M Cunniffe 2, Atul K Garg 3, Maurice N Collins. Regional dependency of bovine meniscus biomechanics on the internal structure and glycosaminoglycan content. Journal of the Mechanical Behavior of Biomedical Materials. 2019, 94, 186-192. https://doi.org/10.1016/j.jmbbm.2019.02.020

[25] Halil L. Tekinalp, Vlastimil Kunc, Gregorio M. Velez-Garcia, Chad E. Duty, Lonnie J. Love, Amit K. Naskar, Craig A. Blue, Soydan Ozcan. Highly oriented carbon fiber–polymer composites via additive manufacturing. Composites Science and Technology. 2014, 105, 144-150. https://doi.org/10.1016/j.compscitech.2014.10.009

[26] Nakagaito, A., Yano, H. The effect of morphological changes from pulp fiber towards nano-scale fibrillated cellulose on the mechanical properties of high-strength plant fiber based composites. Appl Phys A. 2004, 78, 547–552. https://doi.org/10.1007/s00339-003-2453-5

[27] Kelley L. Spence, Richard A. Venditti, Orlando J. Rojas, Youssef Habibi, and Joel J. Pawlak. A comparative study of energy consumption and physical properties of microfibrillated cellulose produced by different processing methods. Cellulose. 2011, 18(4), 1097-1111. https://doi.org/10.1007/s10570-011-9533-z

[28] Takashi Taniguchi, Keizo Okamura. New films produced from microfibrillated natural fibres. Polymer International. 1998, 47(3), 291–294. https://doi.org/10.1002/(SICI)1097-0126(199811)47:3<291::AID-PI11>3.0.CO;2-1

[29] Feng Wang, Taira Hidaka, Hiroshi Tsuno, Jun Tsubota. Co-digestion of polylactide and kitchen garbage in hyperthermophilic and thermophilic continuous anaerobic process. Bioresource Tech. 2012, 112, 67-74. https://doi.org/10.1016/j.biortech.2012.02.064

[30] Mehdi Jonoobi, Jalaludin Harun, Paridah Md. Tahir, Alireza Shakeri, Syeed SaifulAzry, Majid Davoodi Makinejad. Physicochemical characterization of pulp and nanofibers from kenaf stem. Cellulose. 2011, 65(7), 1098-1100. https://doi.org/10.1016/j.matlet.2010.08.054

[31] Ifuku S, Nogi M, Abe K, Handa K, Nakatsubo F, Yano H. Surface modification of bacterial cellulose nanofibers for property enhancement of optically transparent composites: dependence on acetyl-group DS. Biomacromolecules. 2007, 8(6), 1973-8. https://doi.org/10.1021/bm070113b. Epub 2007 Apr 26.

[32] C. Goussé, H. Chanzy, M. L. Cerrada, E. Fleury. Surface silylation of cellulose microfibrils: preparation and rheological properties. Polymer. 2004, 45(5), 1569-1575. https://doi.org/10.1016/j.polymer.2003.12.028

[33] Gilberto Siqueira, Dimitri Kokkinis, Rafael Libanori, Michael K. Hausmann, Amelia Sydney Gladman, Antonia Neels, Philippe Tingaut, Tanja Zimmermann, Jennifer A. Lewis, André R. Studart. Cellulose Nanocrystal Inks for 3D Printing of Textured Cellular Architectures. Advanced Functional Materials. 2017, 27(12). https://doi.org/10.1002/adfm.201604619

[34] Hanna Lönnberg, Linda Fogelström, My Ahmed Said Azizi Samir, Lars Berglund, Eva Malmström, Anders Hult. Surface grafting of microfibrillated cellulose with poly (ε-caprolactone) – Synthesis and characterization. European Polymer Journal. 2008, 44(9), 2991–2997. https://doi.org/10.1016/j.eurpolymj.2008.06.023

[35] S. Valvez, A. P. Silva, P. N. B. Reis, F. Berto. Annealing effect on mechanical properties of 3D printed composites. Procedia Structural Integrity. 2022, 37, 738-745. https://doi.org/10.1016/j.prostr.2022.02.004

[36] Juho Antti Sirviö, Kalle Hyypiö, Shirin Asaadi, Karoliina Junka, Henrikki Liimatainen. High-strength cellulose nanofibers produced via swelling pretreatment based on a choline chloride–imidazole deep eutectic solvent. Green Chemistry. 2020, 22(5), 1763–1775. https://doi.org/10.1039/c9gc04119b

[37] Naoki Tamura, Kota Hasunuma, Tsuguyuki Saito, Shuji Fujisawa. Mechanical and Thermal Properties of Porous Nanocellulose/Polymer Composites: Influence of the Polymer Chemical Structure and Porosity. ACS Omega. 2024, 9(17), 19560–19565. https://doi.org/10.1021/acsomega.4c01206

[38] Aji P. Mathew, Kristiina Oksman, Mohini Sain. Mechanical properties of biodegradable composites from poly lactic acid (PLA) and microcrystalline cellulose (MCC). Journal of Applied Polymer Science. 2005, 97(5), 2014-2025. https://doi.org/10.1002/app.21779

[39] K. Oksman, A. P. Mathew, D. Bondeson, I. Kvien. Manufacturing process of cellulose whiskers/polylactic acid nanocomposites. Composites Science and Technology. 2006, 66(15), 2776-2784. https://doi.org/10.1016/j.compscitech.2006.03.002

[40] Tanja Zimmermann, Nicolae Bordeanu, Esther Strub. Properties of nanofibrillated cellulose from different raw materials and its reinforcement potential. Carbohydrate Polymers. 2010, 79(4), 1086-1093. https://doi.org/10.1016/j.carbpol.2009.10.045

[41] Dieter Klemm, Friederike Kramer, Sebastian Moritz, Tom Lindström, Mikael Ankerfors, Derek Gray, Annie Dorris. Nanocelluloses: A New Family of Nature-Based Materials. 2011, 50(24), 5438-5466. https://doi.org/10.1002/anie.201001273

[42] Moon RJ, Martini A, Nairn J, Simonsen J, Youngblood J. Cellulose nanomaterials review: structure, properties and nanocomposites. Chem Soc. Rev. 2011, 40(7), 3941-94. https://doi.org/10.1039/c0cs00108b

[43] Saleh Hooshmand, Yvonne Aitomäki, Mikael Skrifvars, Aji P Mathew, Kristiina Oksman. All-cellulose nanocomposite fibers produced by melt spinning cellulose acetate butyrate and cellulose nanocrystals. Cellulose. 2014, 21, 2665-2678. https://doi.org/10.1007/s10570-014-0269-4

[44] M A Hubbe, O J Rojas, L A Lucia, M Sain. Cellulosic nanocomposites: a review. BioResources. 2008, 3(3), 929-980. https://doi.org/37878600/BioRes_03_3_0929

[45] Susheel Kalia, Alain Dufresne, Bibin Mathew Cherian, B. S. Kaith, Luc Avérous, James Njuguna, Elias Nassiopoulos. Cellulose-Based Bio- and Nanocomposites: A Review. Int. Journal of Polymer Science. 2011. https://doi.org/10.1155/2011/837875

[46] Abdollah Najafi and Behzad Kord and Ali Abdi and Saeed Ranaee. The impact of the nature of nanoclay on physical and mechanical properties of polypropylene/reed flour nanocomposites. Journal of Thermoplastic Composite Materials. 2012, 25(1), 717-727. https://api.semanticscholar.org/CorpusID:135712778

[47] Sun-Young Lee, Sang-Jin Chun, In-Aeh Kang, Jong-Young Park. Preparation of cellulose nanofibrils by high-pressure homogenizer and cellulose-based composite films. 2009, 15(1), 50-55. https://doi.org/10.1016/j.jiec.2008.07.008

[48] Stephen J Eichhorn, A Dufresne, M Aranguren, N E Marcovich, et al. Current international research into cellulose nanofibres and nanocomposites. Journal of Materials Science. 2010, 45, 1-33. https://doi.org/10.1007/s10853-009-3874-0

[49] H. P. S. Abdul Khalil, A. H. Bhat, A. F. Ireana Yusra. Green composites from sustainable cellulose nanofibrils: A review. Carbohydrate Polymers. 2012, 87(2), 963-979. https://doi.org/10.1016/j.carbpol.2011.08.078

[50] István Sirò & David Plackett. Microfibrillated cellulose and new nanocomposite materials: a review. Cellulose. 2010, 17, 459-494. https://doi.org/10.1007/s10570-010-9405-y

[51] L. Brinchi, F. Cotana, E. Fortunati, J. M. Kenny. Production of nanocrystalline cellulose from lignocellulosic biomass: Technology and applications: Review. Carbohydrate Polymers. 2013, 94(1), 154-169. https://doi.org/10.1016/j.carbpol.2013.01.033